J|A|C|S
ARTICLES
Published on Web 06/03/2004

# Orientational Distribution of CO before and after Photolysis of MbCO and HbCO: A Determination Using Time-Resolved Polarized Mid-IR Spectroscopy

Manho Lim,[†] Timothy A. Jackson,[‡] and Philip A. Anfinrud*[,§]

*Contribution from the Department of Chemistry, Pusan National University, Busan, 609-735, Korea, Harvard-MIT Division of Health Sciences and Technology, Harvard Medical School, Boston, Massachusetts 02115, and Laboratory of Chemical Physics, NIDDK, National Institutes of Health, Bethesda, Maryland 20892*

Received April 4, 2003; E-mail: anfinrud@nih.gov

***Abstract:*** The technique of time-resolved polarized mid-IR spectroscopy was used to probe the orientational distribution of carbon monoxide (CO) bound to and docked within horse myoglobin, sperm whale myoglobin, and human hemoglobin A in neutral pH solution at 283 K. An accurate determination of the orientation required that the experimentally measured polarization anisotropy be corrected for the effects of fractional photolysis in an optically thick sample. The experimental method measures the direction of the transition dipole, which is parallel to the CO bond axis when docked and nearly parallel when bound to the heme. The polarization anisotropy of *bound* CO is virtually the same for all protein systems investigated and is unchanging across its inhomogeneously broadened mid-IR absorption spectrum. From these results, it was concluded that the transition dipole moment of bound CO is oriented $\leq 7°$ from the heme plane normal. The polarized absorbance spectra of *docked* CO are similar for all protein systems investigated, but in stark contrast to bound CO, the polarization anisotropy is strongly correlated with vibrational frequency. The frequency-dependent anisotropy imposes severe constraints on the orientational probability distribution function of the transition dipole, which is well described as a dipole bathed in a Stark field whose out-of-plane motion is constrained by a simple double-well potential. The orientational and spatial constraints imposed on docked CO by the surrounding highly conserved amino acids serve to mediate ligand transport to and from the binding site and thereby control the rates and pathways for geminate ligand rebinding and ligand escape.

## 1. Introduction

It is well-known that the amino acid side chains arrayed about the active site of an enzyme strongly influence its reactivity and selectivity. To gain insight into the functional role of these side chains, it is crucial to know the structures of enzyme−substrate intermediates involved in the reaction. In some cases, reaction intermediates can be studied by trapping at low temperatures.[1−7] When freezing an enzyme, one runs the risk of halting conformational changes that may be crucial to the function of that enzyme. It would be preferable, whenever possible, to pursue studies under more physiologically relevant conditions. The experimental challenges posed by such studies are significant. However, for a growing number of systems, in particular for ligand-binding heme proteins such as carbon monoxy-myoglobin (MbCO), those challenges are being surmounted. Indeed, short-lived intermediates of a photolyzed mutant of MbCO have now been structurally characterized with 150 ps time-resolved X-ray crystallography.[8] While time-resolved X-ray crystallography can lead to new insights into the function of a protein, those insights can be deepened significantly through complementary spectroscopic investigations.[8]

The physiological functions of Mb and Hb are, respectively, to store and transport $O_2$. In both cases, the active binding site is an Fe(II)-containing porphyrin group (ferrous heme) that is confined within the hydrophobic interior of the protein. In the deoxy state, i.e., without a bound ligand, the heme is coordinated to four equatorial nitrogens from the porphyrin and one axial nitrogen from the proximal histidine (see Figure 1). The sixth coordination site on the distal side of the heme is available to

[†] Department of Chemistry, Pusan National University.
[‡] Harvard-MIT Division of Health Sciences and Technology, Harvard Medical School.
[§] Laboratory of Chemical Physics, NIDDK, National Institutes of Health.

(1) Schlichting, I.; Berendzen, J.; Phillips, G. N., Jr.; Sweet, R. M. *Nature* **1994**, *371*, 808−812.
(2) Teng, T. Y.; Srajer, V.; Moffat, K. *Nat. Struct. Biol.* **1994**, *1*, 701−705.
(3) Hartmann, H.; Zinser, S.; Komninos, P.; Schneider, R. T.; Nienhaus, G. U.; Parak, F. *Proc. Natl. Acad. Sci. U.S.A.* **1996**, *93*, 7013−7016.
(4) Teng, T. Y.; Srajer, V.; Moffat, K. *Biochemistry* **1997**, *36*, 12 087−12 100.
(5) Brunori, M.; Vallone, B.; Cutruzzola, F.; Travaglini-Allocatelli, C.; Berendzen, J.; Chu, K.; Sweet, R. M.; Schlichting, I. *Proc. Natl. Acad. Sci. U.S.A.* **2000**, *97*, 2058−2063.
(6) Chu, K.; Vojtchovsky, J.; McMahon, B. H.; Sweet, R. M.; Berendzen, J.; Schlichting, I. *Nature* **2000**, *403*, 921−923.
(7) Ostermann, A.; Waschipky, R.; Parak, F. G.; Nienhaus, G. U. *Nature* **2000**, *404*, 205−208.
(8) Schotte, F.; Lim, M.; Jackson, T. A.; Smirnov, A.; Soman, J.; Olson, J. S.; George N. Phillips, J.; Wulff, M.; Anfinrud, P. A. *Science* **2003**, *300*, 1944−1947.


**10.1021/ja035475f CCC: $27.50** 

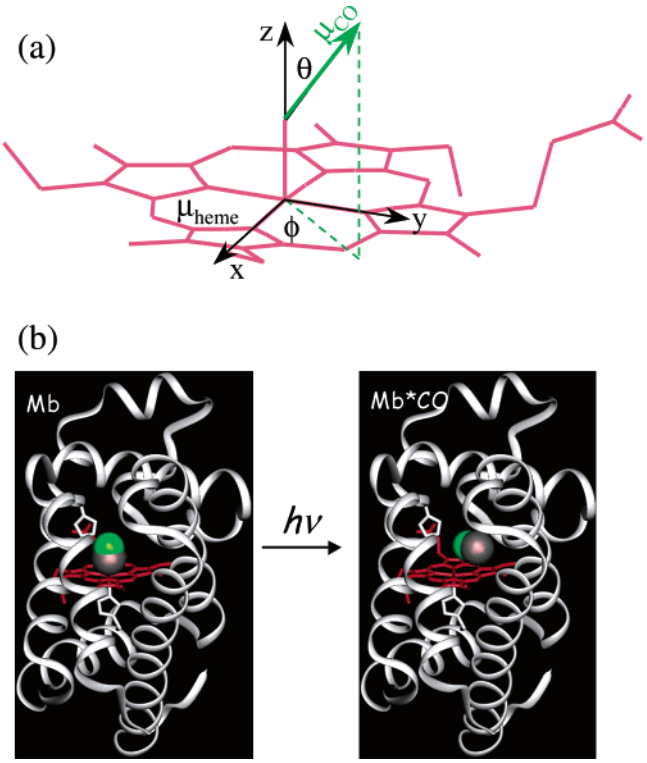


***Figure 1.*** (a) Heme-CO coordinate system: $\theta$ is the angle between the CO bond and the heme plane normal; $\phi$ is the azimuthal angle around the heme plane normal. (b) Structures of MbCO and photolyzed carbonmonoxy myoglobin (Mb*CO).

reversibly bind other small ligands such as $O_2$, CO, and NO. The free energy of ligand binding has been tuned by Mb and Hb to optimize their respective physiological functions. For example, Mb has a higher affinity for $O_2$ than Hb,[9] thereby facilitating the diffusion of $O_2$ from Hb in the blood to Mb in the tissues. Moreover, Hb is a tetrameric protein that cooperatively binds up to four ligands: cooperativity arises from a ligand-induced quaternary conformational change that increases the binding affinity of the hemes as they become fully saturated.[10] This cooperative binding enhances the efficiency by which Hb acquires $O_2$ from the lungs and delivers it to the tissues. In addition to modulating the binding affinity for $O_2$, the protein surrounding the heme in both Mb and Hb serves to discriminate between $O_2$ and CO. For example, CO binds to protein-free heme in organic solvents about $10^3$ to $10^4$ times as strongly as $O_2$,[11] but binds to Mb and Hb approximately 30 and 200 times as strongly as $O_2$,[9] respectively. This discrimination is important: given the level of inhibition afforded by the protein, CO produced endogenously by the metabolism of heme poisons only about 1% of the Hb and Mb in humans.[12]

The methods exploited by Nature to tune the heme-ligand binding affinity and geminate rebinding rates has been the subject of numerous investigations spanning many decades. Owing to their chemical stability and photolyzability, carbon monoxy-heme proteins have long served as model systems for investigating spectroscopic and structural intermediates along the ligand binding and escape pathways. For example, when MbCO is photolyzed, CO is excreted into the surrounding solvent with high efficiency (only around 4% geminately rebinds at room temperature).[13] When HbCO is photolyzed, approximately 50% of the dissociated CO geminately rebinds.[14,15] Previous ultrafast time-resolved mid-IR studies of photolyzed MbCO and HbCO sought to characterize the orientation of bound and dissociated CO, and uncovered evidence for a ligand docking site[16] near the heme binding site that constrains the orientation of the docked ligand to lie in the plane of the heme.[17,18] Because this orientation is far from the transition state for binding, the interactions that constrain CO contribute to its remarkably efficient expulsion from MbCO. Low-temperature X-ray structures of photolyzed MbCO reveal an ellipsoidal electron density for "docked" CO located ~1−2 Å from the heme normal,[1−4] whose major axis is nominally aligned with the heme plane. A displacement of this magnitude is also consistent with an EXAFS study of MbCO photolyzed at 10 K.[19] The close proximity of the docking site to the binding site explains the rapid sub-ps development of the "docked" features[18] and the high efficiency for ligand trapping in that site. Earlier time-resolved polarized mid-IR studies of the docked state in MbCO revealed tantalizing features in the polarization anisotropy that required further effort to interpret in detail. In this paper, we extend our earlier work on *sw*-MbCO to include other related protein systems, and interpret the polarized mid-IR spectra of "docked" CO with a Stark-field model that leads to a detailed and robust determination of its orientational probability distribution function.

## 2. Relations between CO Orientation and Polarization Anisotropy

When a solution of MbCO or HbCO is photolyzed with a linearly polarized visible pulse, those hemes whose transition dipole moments happen to be oriented along the photolysis polarization direction absorb light most efficiently (in the small signal limit, the absorption probability is proportional to $\cos^2\alpha$ where $\alpha$ is the angle between the polarization vector and the transition dipole moment of the heme). Consequently, a linearly polarized photolysis pulse creates an anisotropic distribution of photoexcited hemes. The CO molecules bound to these "photoselected" hemes are dissociated, thereby creating an anisotropic distribution of bound and "docked" CO. The wavelength-dependent polarization anisotropy

$$r(\lambda) = \frac{\Delta A^{\parallel}(\lambda) - \Delta A^{\perp}(\lambda)}{\Delta A^{\parallel}(\lambda) + 2\Delta A^{\perp}(\lambda)} \qquad (1)$$

can be calculated from the pump-induced change in the CO absorbance spectra measured parallel ($\Delta A^{\parallel}$) and perpendicular

(9) Antonini, E.; Brunori, M. *Hemoglobin and Myoglobin in Their Reactions With Ligands*; North-Holland Publishing Company: London, 1971.
(10) Perutz, M. *Mechanisms of Cooperativity and Allosteric Regulation in Proteins*; Cambridge University Press: Cambridge, UK, 1990.
(11) Collman, J. P.; Brauman, J. I.; Halbert, T. R.; Suslick, K. S. *Proc. Natl. Acad. Sci. U.S.A.* **1976**, *73*, 3333−3337.
(12) Coburn, R. F. *Ann. N. Y. Acad. Sci.* **1970**, *174*, 11−22.
(13) Henry, E. R.; Sommer, J. H.; Hofrichter, J.; Eaton, W. A. *J. Mol. Biol.* **1983**, *166*, 443−451.
(14) Murray, L. P.; Hofrichter, J.; Henry, E. R.; Ikeda-Saito, M.; Kitagishi, K.; Yonetani, T.; Eaton, W. A. *Proc. Natl. Acad. Sci. U.S.A.* **1988**, *85*, 2151−2155.
(15) Murray, L. P.; Hofrichter, J.; Henry, E. R.; Eaton, W. A. *Biophys. Chem.* **1988**, *29*, 63−76.
(16) Lim, M.; Jackson, T. A.; Anfinrud, P. A. *J. Chem. Phys.* **1995**, *102*, 4355−4366.
(17) Lim, M.; Jackson, T. A.; Anfinrud, P. A. *Science* **1995**, *269*, 962−966.
(18) Lim, M.; Jackson, T. A.; Anfinrud, P. A. *Nat. Struct. Biol.* **1997**, *4*, 209−214.
(19) Chance, M. R.; Miller, L. M.; Fischetti, R. F.; Scheuring, E.; Huang, W.-X.; Sclavi, B.; Hai, Y.; Sullivan, M. *Biochemistry* **1996**, *35*, 9014−9023.

($\Delta A^{\perp}$) to the photolysis polarization direction. When photolyzed at a wavelength where the heme possesses a 2-fold degenerate transition dipole in its plane (i.e., the heme is a circular absorber), $r$ can theoretically span the range $-0.2 \le r \le 0.1$, and the measured anisotropy can impose stringent constraints on the angle between the CO transition dipole moment and the heme normal, i.e., the angle $\theta$ in Figure 1a. Note that these polarization anisotropy measurements average over the azimuthal angle, $\phi$, making them insensitive to $\phi$. Nonetheless, as we demonstrate in this paper, the measured polarization anisotropy "spectrum" imposes stringent constraints on the orientation and orientational distribution of both bound and "docked" CO.

**2.1 Orientation of bound CO.** When CO is bound to the heme of Mb or Hb, its chemical linkage imposes severe constraints on the direction of its transition dipole moment. If oriented at an angle $\theta$ with respect to the heme normal, and if its orientational probability distribution function, $P(\theta)$, is a delta function in $\theta$, then

$$\theta = \sin^{-1}\sqrt{(10/3)(r + 0.2)} \qquad (2)$$

where the range $-0.2 \le r \le 0.1$ corresponds to $0° \le \theta \le 90°$.[20,21] (For the special case when $r = 0$, the transition dipole moment of CO is either oriented isotropically or is oriented 54.7° relative to the heme plane normal, the so-called "magic" angle.) Equation 2 must be used with caution because $P(\theta)$ is not a delta function but has a shape and width that arises from thermal motion on a complex multidimensional potential energy surface. The broader the distribution in $\theta$, the smaller the absolute magnitude of the measured anisotropy, even if the equilibrium orientation remains unchanged. Consequently, a definitive determination of the equilibrium CO orientation, $\theta_{eq}$, requires knowledge of the orientational probability distribution function. For example, when P($\theta$) is known, $\theta_{eq}$ can be estimated from eq 2 by substituting ($r$/$S$) for $r$,[22] where $S$ is an order parameter ($0 < S \le 1$) related to P($\theta$)[23] through

$$S = \frac{\frac{1}{2}\int_0^{\pi}(3\cos^2\theta' - 1)P(\theta')\sin\theta' d\theta'}{\int_0^{\pi}P(\theta')\sin\theta' d\theta'} \qquad (3)$$

In this notation, $\theta'$ refers to the angular displacement relative to the equilibrium orientation, $\theta_{eq}$. Note that when the measured anisotropy approaches the limit of $-0.2$, the order parameter must approach 1, and the equilibrium orientation, $\theta_{eq}$, approaches 0. In this work, the measured polarization anisotropy of CO bound to Mb and Hb approaches the theoretical limit of $-0.2$, thereby imposing stringent constraints on the orientation and orientational distribution of the CO transition dipole.

**2.2 Orientation of "Docked" CO.** The orientation of "docked" CO would be best defined in terms of its orientational probability distribution function. The shape of this function can be deduced from polarized CO vibrational absorbance spectra. This determination is possible because "docked" CO is bathed in a static electric field, which leads to an orientation-dependent Stark shift of its vibrational frequency.[24−26] The vibrational Stark shift arises from the change of dipole moment associated with a vibrational transition and is proportional to $-\mathbf{E}\cdot\Delta\mu$,[24,26−28] where $\mathbf{E}$ is the electric field sensed by the CO molecule and $\Delta\mu$ is the Stark tuning rate.[26−29] Because $\Delta\mu$ is opposed to the permanent $C^-O^+$ dipole,[25,29] the vibrational frequency is maximally blue shifted when $\Delta\mu$ is parallel to $\mathbf{E}$ (when the O end of CO points in the direction of the E-field vector). The Stark tuning rate of docked CO in a frozen glass was measured and found to be 67 $cm^{-1}(V/Å)^{-1}$ (equivalently 0.04 D).[26] Given this tuning rate, a 0.2 V/ Å electrostatic field in the vicinity of the heme pocket docking site (estimated theoretically) [30] would produce a vibrational Stark shift of around 13 $cm^{-1}$, which is greater than the vibrational line width of CO. Therefore, the spectrum of "docked" CO would be expected to exhibit an orientation-dependent Stark shift as well as a frequency-dependent polarization anisotropy.

To experimentally observe this spectroscopic inhomogeneity, the "docked" CO must sample its accessible range of orientations on a time scale that is slow compared to its vibrational dephasing time. (The vibrational dephasing time for "docked" CO is not known, but is probably no faster than that for bound CO, whose ambient temperature dephasing time is ~4 ps.[31,32]) This condition appears to be met: the vibrational spectrum of "docked" CO reveals two well-defined features that appear to arise from a Stark splitting,[16] and its polarization anisotropy is vibration-frequency dependent.[17]

The simplest model that can account for the vibrational splitting and the frequency-dependent polarization anisotropy is based on a cylindrically symmetric double-well potential written in spherical polar coordinates

$$V(\theta,\phi) = V_0\left(\frac{1}{\sin^2(0.5 \times \cos^{-1}(\hat{r}(\theta,\phi)\cdot\hat{r}(\theta_1,\phi_1)))} + \frac{1}{\Delta + \sin^2(0.5 \times \cos^{-1}(\hat{r}(\theta,\phi)\cdot\hat{r}(\theta_2,\phi_2)))}\right)^{-1} \qquad (4)$$

where $\hat{r}(\theta_1,\phi_1)$ and $\hat{r}(\theta_2,\phi_2)$ are the unit direction vectors for the equilibrium orientation of CO in the two wells, $V_0$ is related to the potential barrier separating the two wells, and $\Delta$ is the energy difference between the two minima. Given eq 4 and a Boltzmann distribution of thermal energies, the orientational probability distribution function is computed from

$$P(\theta,\phi) \propto \exp\left(-\frac{V(\theta,\phi)}{RT}\right)$$

This function looks like a bent "peanut" with two lobes of high probability oriented in different directions (see Figure 2 for

(20) Ormos, P.; Braunstein, D.; Frauenfelder, H.; Hong, M. K.; Lin, S. L.; Sauke, T. B.; Young, R. D. *Proc. Natl. Acad. Sci. U.S.A.* **1988**, *85*, 8492−8496.
(21) Moore, J. N.; Hansen, P. A.; Hochstrasser, R. M. *Proc. Natl. Acad. Sci. U.S.A.* **1988**, *85*, 5062−5066.
(22) Ansari, A.; Szabo, A. *Biophys. J.* **1993**, *64*, 838−851.
(23) Bocian, D. F.; Chan, S. I. *Annu. Rev. Phys. Chem.* **1978**, *29*, 307−335.
(24) Augspurger, J. D.; Dykstra, C. E.; Oldfield, E. *J. Am. Chem. Soc.* **1991**, *113*, 2447−2451.
(25) Ma, J.; Huo, S.; Straub, J. E. *J. Am. Chem. Soc.* **1997**, *119*, 2541−2551.
(26) Park, E. S.; Boxer, S. G. *J. Phys. Chem. B* **2002**, *106*, 5800−5806.
(27) Reimers, J. R.; Hush, N. S. *J. Phys. Chem. A* **1999**, *103*, 10 580−10 587.
(28) Andrews, S. S.; Boxer, S. G. *J. Phys. Chem. A* **2002**, *106*, 469−477.
(29) Park, E. S.; Andrews, S. S.; Hu, R. B.; Boxer, S. G. *J. Phys. Chem. B* **1999**, *103*, 9813−9817.
(30) McMahon, B. H.; Stojkovic, B. P.; Hay, P. J.; Martin, R. L.; Garcia, A. E. *J. Chem. Phys.* **2000**, *113*, 6831−6850.
(31) Rella, C. W.; Rector, K. D.; Kwok, A.; Hill, J. R.; Schwettman, H. A.; Dlott, D. D.; Fayer, M. D. *J. Phys. Chem.* **1996**, *100*, 15 620−15 629.
(32) Lim, M.; Hamm, P.; Hochstrasser, R. M. *Proc. Natl. Acad. Sci. U. S. A.* **1998**, *95*, 15 315−15 320.

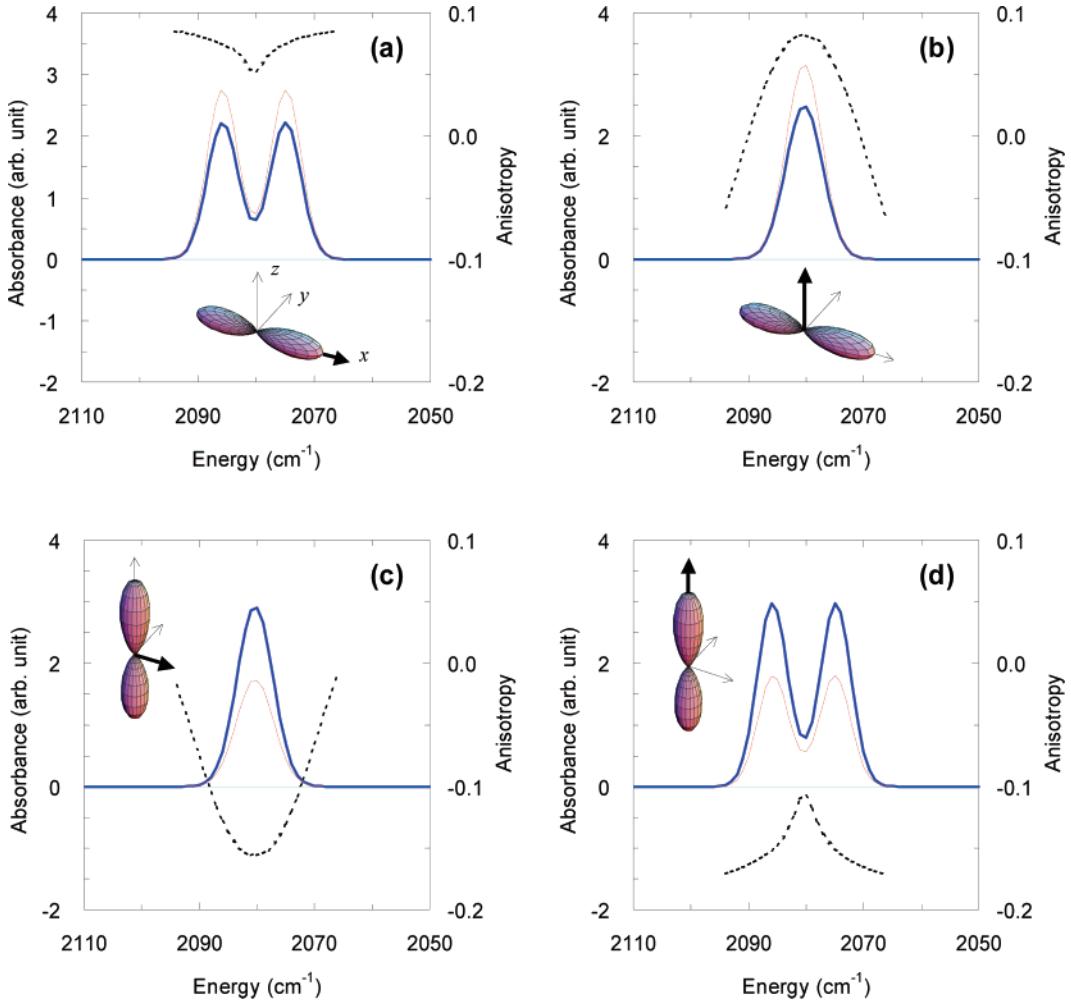


***Figure 2.*** Polarized absorbance (thin lines, $\Delta A^{\parallel}$; thick lines, $\Delta A^{\perp}$) and anisotropy (dashed lines) predicted with CO trapped in a double well cosine $\theta$ potential while bathed in a Stark field. Here, the parameters in eq 4 are chosen to produce peanut-like distributions with the population distributed equally in the two lobes ($\Delta = 0$). The polarized spectra and its anisotropy are quite sensitive to the direction of the Stark field (boldface arrow) and the direction of the orientational probability distribution function (plotted as a 3-D rendered object). The *z*-axis is parallel to the heme normal. When the Stark field is aligned along the long axis of the orientational probability distribution function (panels **a** and **d**), the "docked" CO absorbance splits into two bands. When the Stark field and the long axis of the orientational probability distribution function are both parallel to the heme plane (panel **a**), the polarized absorbance and its anisotropy are qualitatively similar to that which is observed experimentally (compare panel **a** with *B*-states of Figure 5).

limiting case where the lobes are oriented oppositely). Given this orientational probability distribution function, Stark-shifted polarized vibrational spectra and their polarization anisotropy can be calculated numerically and compared with their experimentally determined counterparts. If the long axis of the "peanut" is oriented parallel to the E-field, the vibrational spectrum will be maximally split into two features (see Figure 2a,d). If the E-field is aligned perpendicular to the long axis, there will be no splitting, only a broadening of the vibrational spectrum (see Figure 2b,c). The vibrational spectrum, therefore, imposes constraints on the breadth of the orientational probability distribution function as well as the relative direction of the E-field. The frequency dependence of the polarization anisotropy imposes additional constraints on the direction of the E-field as well as on the direction vector of the orientational probability distribution function (relative to the heme normal). The geometric constraints imposed by the vibrational spectrum *and* its anisotropy on the orientational probability distribution function and the E-field direction are quite stringent, allowing the parameters of this model to be robustly determined. Because the polarization anisotropy measurements average over the azimuthal angle, the $\phi$ angle of the orientational probability distribution is indeterminate. Moreover, because polarization anisotropy measurements probe the magnitude of the projection of the orientational probability distribution function on the heme normal, we cannot distinguish between up and down directions.

**2.3 Anisotropy Correction in an Optically Thick Sample.** To determine the mid-IR polarization anisotropy of CO with an acceptable signal-to-noise ratio, a reasonable fraction of the sample must be photolyzed. Because the pump-induced change of the parallel-polarized absorbance spectrum saturates more quickly than its perpendicular polarized counterpart, the magnitude of the anisotropy determined using eq 1 decreases as the photolysis level increases. Indeed, as the level of photolysis approaches 100%, $\Delta A^{\parallel}$ and $\Delta A^{\perp}$ converge to the same value and the anisotropy approaches zero. Clearly, to determine the orientation of CO from its measured anisotropy, the anisotropy must be deduced in the limit of zero photolysis. The polarization anisotropy in this limit, $r_{lim}$, can be calculated by dividing the experimentally determined anisotropy, $r_{exp}$, by a photolysis-level-dependent correction factor.[22,33] Using the

notation of Ansari and Szabo[22]

$$r_{\mathrm{lim}} = \frac{r_{\mathrm{exp}}}{\left(\frac{a_2}{1 - a_0}\right)} \tag{5}$$

where

$$a_0 = \int_0^1 \exp(-\epsilon I_0(1 - \sigma P_2(x)))\, dx$$

$$a_2 = 5\int_0^1 P_2(x)\, \exp(-\epsilon I_0(1 - \sigma P_2(x)))dx$$

The term $(1 - a_0)$ is the fraction of molecules photolyzed by the pump pulse and $a_2$ is proportional to the linear dichroism induced by linear polarized excitation of an isotropic system. $I_0$ is the time integral of the photolysis pulse intensity over the duration of that pulse, $\epsilon$ is the isotropic extinction coefficient at the photolysis wavelength, $\sigma = 1$ for a circular absorber, $P_2(x)$ is the second-order Legendre polynomial, and $x = \cos\theta$.

The correction factor in eq 5 applies to optically *thin* samples, i.e., the fraction of molecules photolyzed remains uniform as the photolysis pulse passes through the sample. The samples used in this study were optically *thick* with absorbances of approximately 1.5 for *h*-MbCO, 1.4 for *sw*-MbCO and 1.8 for HbCO at 527 nm. These high concentrations were required to compensate for the small absolute intensity of the CO vibrational spectrum. For *sw*-MbCO, an average photolysis of 10% (20%) leads to 30% (50%) photolysis at the front of the sample and only 2% (2.5%) at the rear of the sample. Clearly, studies carried out under these conditions mandate that we determine the correction factor for optically *thick* samples.

We have shown that the appropriate correction factor for an optically *thick* sample can be calculated as a sum over optically *thin* ones, with parameters in each optically *thin* slice determined according to the fraction of molecules photolyzed within that slice, i.e.

$$\sum_i (\{a_{2,i}\}/(1 - a_{0,i}))f_i$$

where $i$ is the index for each slice and $f_i$ is its fractional contribution to the total number of photolyzed molecules.[34] Calculation of the degree of photolysis within each optically *thin* slice must account for the absorbance of the sample at the photolysis wavelength ($A$; corresponding to MbCO or HbCO), the absorbance of a completely photolyzed sample at the same wavelength ($A^*$; corresponding to Mb or Hb), and the average degree of photolysis within that slice. The absorbance of the photoproduct, $A^*$, is required because its absorbance affects the penetration depth of the photolysis pulse. It should be noted that if the photolysis pulse is sufficiently short in duration, $A^*$ corresponds to the excited-state absorbance of the sample, not the ground-state absorbance of the photoproduct. The correction factor becomes a strong function of $A$ and $A^*$ at higher levels of photolysis, thereby causing the optically thick correction factor to differ significantly from the optically thin limit ($A \rightarrow 0$).[34]

## 3. Experimental Section

**3.1 Sample Preparation.** Human hemoglobin A was prepared from the hemolysate of fresh red blood cells[9] and purified by chromatography on a DEAE-Sephacel column. The solution was dialyzed against $D_2O$ buffered with 0.1 M potassium phosphate, pD 7.5. The $HbO_2$ was converted to HbCO by stirring under 1 atm of CO for 12 h. The final concentration of HbCO was ~4 mM.

Horse myoglobin was prepared by dissolving lyophilized skeletal horse myoglobin (Sigma) in deoxygenated $D_2O$ buffered with 0.1 M potassium phosphate, pD 7.5, or deoxygenated 75% glycerol/water (v/v) buffered with 0.1 M potassium phosphate, pH 7.1. The solutions were equilibrated with 1 atm of CO and the metaquo Mb was reduced with an equimolar concentration of sodium dithionite. The final concentration of *h*-MbCO was ~14 mM.

Sperm whale myoglobin was received in solution form: ~10 mM *sw*-MbCO in $D_2O$ buffered with 0.1 M potassium phosphate, pD 7.5. To exchange $^{13}CO$ for $^{12}CO$, the MbCO was first converted to Mb by purging with $N_2$ for 4 h while the surface of the stirred solution was illuminated with ~1W of visible light from an $Ar^+$ laser. After removal of the CO, the Mb solution was equilibrated with 1 atm $^{13}CO$. An equimolar amount of sodium dithionite was added to ensure that all the Mb was in the ferrous form. The solution was concentrated to ~14 mM by centrifugation at 5000 g in a Centricon-10 concentrator.

Because the mid-IR transmission of $D_2O$ drops dramatically to the blue of 2100 $cm^{-1}$, all samples prepared in $D_2O$ were liganded with $^{13}CO$, thereby shifting the unbound CO spectrum into a region with greater IR transmission. There is no such advantage when 75% glycerol/water (v/v) is used as a solvent, so samples prepared in G/W were liganded with $^{12}CO$.

All samples were centrifuged at 5000 g for 15 min. prior to loading into gastight 0.1 mm path length sample cells with $CaF_2$ windows.

**3.2 Time-Resolved Mid-IR Spectrometer.** We have developed an ultrafast time-resolved mid-IR absorption spectrometer that achieves high sensitivity, ultrafast time resolution, and tunability over 3.3−5.5 $\mu$m. The details of this spectrometer are described elsewhere.[16,35] Briefly, a pump pulse photolyzed the sample and its transient mid-IR absorbance was probed with an optically delayed, sub-200 fs mid-IR probe pulse. To attain the spectral resolution needed to record the vibrational spectrum of CO, the broadband transmitted mid-IR probe pulse was routed through an IR monochromator and a 3 $cm^{-1}$ spectral slice was detected with an amplified $N_2(l)$-cooled InSb photodetector (EG&G). The 250 $cm^{-1}$ bandwidth of the probe and the fine spectral resolution of the monochromator allowed spectra to be measured over a broad spectral range with a wavelength accuracy of $\pm$0.2 $cm^{-1}$. To record the sample transmission, the signal was normalized with respect to a reference mid-IR pulse that was routed through the same monochromator and detected with a matched IR photodetector. The pump-induced change in the absorbance of the sample was determined by chopping the pump pulse at half the repetition frequency of the laser and computing the difference between the pumped and unpumped absorbance. Signal averaging at the 1.5-kHz repetition frequency of the laser reduced the noise level to $< 2 \times 10^{-4}$ in absorbance units after 1 s of signal averaging. Mid-IR spectra spanning 100 $cm^{-1}$ were scanned in 1 $cm^{-1}$ steps in less than 3 min. The spectra reported here represent the average of ~15 and ~60 scans for bound and docked CO, respectively. With this amount of signal averaging, the noise level of the docked CO spectra was reduced to less than $\sim 3 \times 10^{-5}$ in absorbance units.

The samples were photolyzed with 35ps, 527 nm pulses. At this wavelength, the heme is a circular absorber[36] and the relationship between polarization anisotropy and CO orientation is simplified. The pump and probe pulses were focused to ~250 $\mu$m and ~150 $\mu$m

(33) Hansen, P. A.; Moore, J. N.; Hochstrasser, R. M. *Chem. Phys.* **1989**, *131*, 49−62.
(34) Lim, M. *Bul. Kor. Chem. Soc.* **2002**, *23*, 865−871.
(35) Anfinrud, P. A.; Lim, M.; Jackson, T. A. *Proc. SPIE-Int. Soc. Opt. Eng. (Longer Wavelength Lasers and Applications)* **1994**, *2138*, 107−115.
(36) Eaton, W. A.; Hofrichter, J. *Methods Enzymol.* **1981**, *76*, 175−261.

diameter spots, respectively. The pump spot was made significantly larger than the probe spot to ensure spatially uniform photolysis across the spatial dimensions of the probe pulse. The pump−probe optical delay was set to 100 ps. This delay is long compared to the 6 ps thermal relaxation time of the photolyzed protein[37] and the 35 ps pump pulse duration, but is short compared to the several hundred ns time for ligand escape from the docking site[17] and the rotational diffusion times of the protein.[38,39] Rotational diffusion of the protein randomizes the orientation of the photoselected hemes and causes the polarization anisotropy to decay to zero. Consequently, a precise determination of the CO orientation requires that its polarization anisotropy be measured at a time that is short compared to the rotational diffusion time of 8 ns for Mb at 288 K[38] and 26 ns for Hb at 293 K[39]). Note that at the elevated protein concentrations used in this investigation, the solution is more viscous and the rotational diffusion is considerably slower: the rotational diffusion times for Mb in $D_2O$, Mb in G/W and Hb in $D_2O$ at 283 K were found to be 55 ns, 2.6 $\mu$s and 144 ns, respectively. This experimental determination was made by recording the decay of the measured polarization anisotropy after excitation with an electronically delayed 5 ns, 527 nm pump pulse.

Transient mid-IR spectra of bound CO were recorded at approximately 10% photolysis, which required approximately 1.5 $\mu$J of pump pulse energy. The spectra of docked CO were recorded at approximately 20% photolysis. The sample cell was rotated sufficiently fast to provide a fresh sample for each photolysis pulse. The rotating sample cell was enclosed in a home-built refrigerator and maintained at 10 °C.

During a wavelength scan, the polarization of the photolysis pulse was alternated between parallel and perpendicular orientations using a computer-controlled liquid-crystal retarder (Meadowlark). This device facilitated measurement of both polarized spectra nearly simultaneously and afforded greater immunity to instrumental drift. Special care was taken to ensure that both polarizations were pure (extinction ratios were routinely better than 1000:1) and of equal intensity (after reflecting off an aluminum mirror, the perpendicular polarization was ≈ 0.8% more intense than the parallel polarization; the data were corrected accordingly).

## 4. Results and Discussion

**4.1 Validation of Anisotropy Correction in an Optically Thick Sample.** In Section 2.3, we outlined an approach for determining the polarization anisotropy in the zero-photolysis limit, $r_{lim}$, from the anisotropy measured under finite photolysis conditions in an optically thick sample. To test this approach, we measured the polarization anisotropy of CO bound to the heme of *sw*-Mb at various levels of photolysis. At the photolysis wavelength of 527 nm, this MbCO sample had an optical density $A = 1.4$ (if fully converted to its photoproduct, Mb, it would have an absorbance of $A^* = 1.1$). As expected, the magnitude of the polarization anisotropy decreases monotonically with increasing level of photolysis (see Figure 3). The trend is well described by the thick line, whose zero-photolysis limit is $r_{lim} = -0.191_8$. To obtain this estimate, the data were least-squares fit with $r_{lim}$ as the only free parameter. According to this curve, the polarization anisotropy measured at 20% photolysis would be $r = -0.172_6$. If we had made a measurement at that level of photolysis and assumed that our sample was optically *thin*,[22,33] the extrapolation to zero photolysis would yield $r_{lim} = -0.183_2$, which underestimates the correct value by nearly 5%. In the limit that $P(\theta)$ is a delta function, the orientation of CO corresponding to $r_{lim} = -0.183_2$ (optically *thin*) and $-0.191_8$ (optically *thick*) is $\theta_{lim} = 13.7°$ and 9.5°, respectively. Clearly, ignoring the effects of an optically thick sample can influence significantly the orientation calculated for CO. All anisotropies reported here have been corrected according to this protocol.

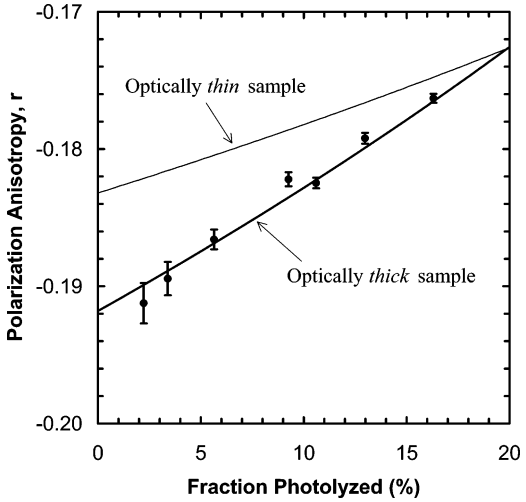


***Figure 3.*** Polarization anisotropy measured as a function of the average level of photolysis within an optically thick sample. The filled circles correspond to the anisotropy measured for *sw*-Mb$^{13}$CO:$D_2O$ at various levels of photolysis. The error bars correspond to one standard deviation. The thick line corresponds to the predicted polarization anisotropy of an optically *thick* sample, whose zero-photolysis limit is $r_{lim} = -0.191_8$. For comparison, the thin line depicts the extrapolation for an optically *thin* sample measured at 20% photolysis.

**4.2 Time-Resolved Polarized Mid-IR Spectra.** Time-resolved polarized mid-IR absorbance spectra of photolyzed *h*-MbCO, *sw*-MbCO, and HbCO are shown in Figure 4. The negative- and positive-going features are denoted *A*- and *B*-states, respectively, following the convention of Alben et al.[40] The *A*-states retrace the equilibrium IR spectra of MbCO and HbCO and correspond to the photolysis-induced depletion of bound CO. The *B*-states correspond to CO dissociated from the heme iron but trapped within a docking site in the protein.[16−18]

**4.3 A-State Anisotropy: Orientation of Bound CO.** As reported previously, the *A*-state spectrum of photolyzed HbCO is dominated by one prominent feature.[16] In contrast, the *A*-state spectra of *h*-MbCO and *sw*-MbCO reveal two features, a main band ($A_1$) and a shoulder ($A_3$).[41] It had been suggested that multiple *A*-states arise from multiple conformations of the protein, each of which can have a different CO orientation.[20,21,42] According to Figure 4, the polarization anisotropy is virtually constant across $A_1$ and $A_3$, with the scatter of the data corresponding to an angular dispersion of only ∼± 1.1°. Moreover, the measured anisotropy is virtually identical across all four samples investigated, whose weighted average in the zero-photolysis limit, $\langle r_{lim} \rangle$, is summarized in Table 1. This constancy in the anisotropy suggests that splitting of the *A*-state arises not from different CO orientations, but from conforma-

(37) Lim, M.; Jackson, T. A.; Anfinrud, P. A. *J. Phys. Chem.* **1996**, *100*, 12 043−12 051.
(38) Albani, J.; Alpert, B. *Chem. Phys. Lett.* **1986**, *131*, 147−152.
(39) McKalley, R. C.; Shimshick, E. J.; McConnell, H. M. *Chem. Phys. Lett.* **1972**, *13*, 115−119.
(40) Alben, J. O.; Beece, D.; Bowne, S. F.; Doster, W.; Eisenstein, L.; Frauenfelder, H.; Good, D.; McDonald, J. D.; Marden, M. C.; Mo, P. P.; Reinisch, L.; Reynolds, A. H.; Shyamsunder, E.; Yue, K. T. *Proc. Natl. Acad. Sci. U.S.A.* **1982**, *79*, 3744−3748.
(41) Ansari, A.; Berendzen, J.; Braunstein, D. K.; Cowen, B. R.; Frauenfelder, H.; Hong, M. K.; Iben, I. E. T.; Johnson, J. B.; Ormos, P.; Sauke, T. B.; Scholl, R.; Schulte, A.; Steinbach, P. J.; Vittitow, J.; Young, R. D. *Biophys. Chem.* **1987**, *26*, 337−355.
(42) Kuriyan, J.; Wilz, S.; Karplus, M.; Petsko, G. A. *J. Mol. Biol.* **1986**, *192*, 133−154.

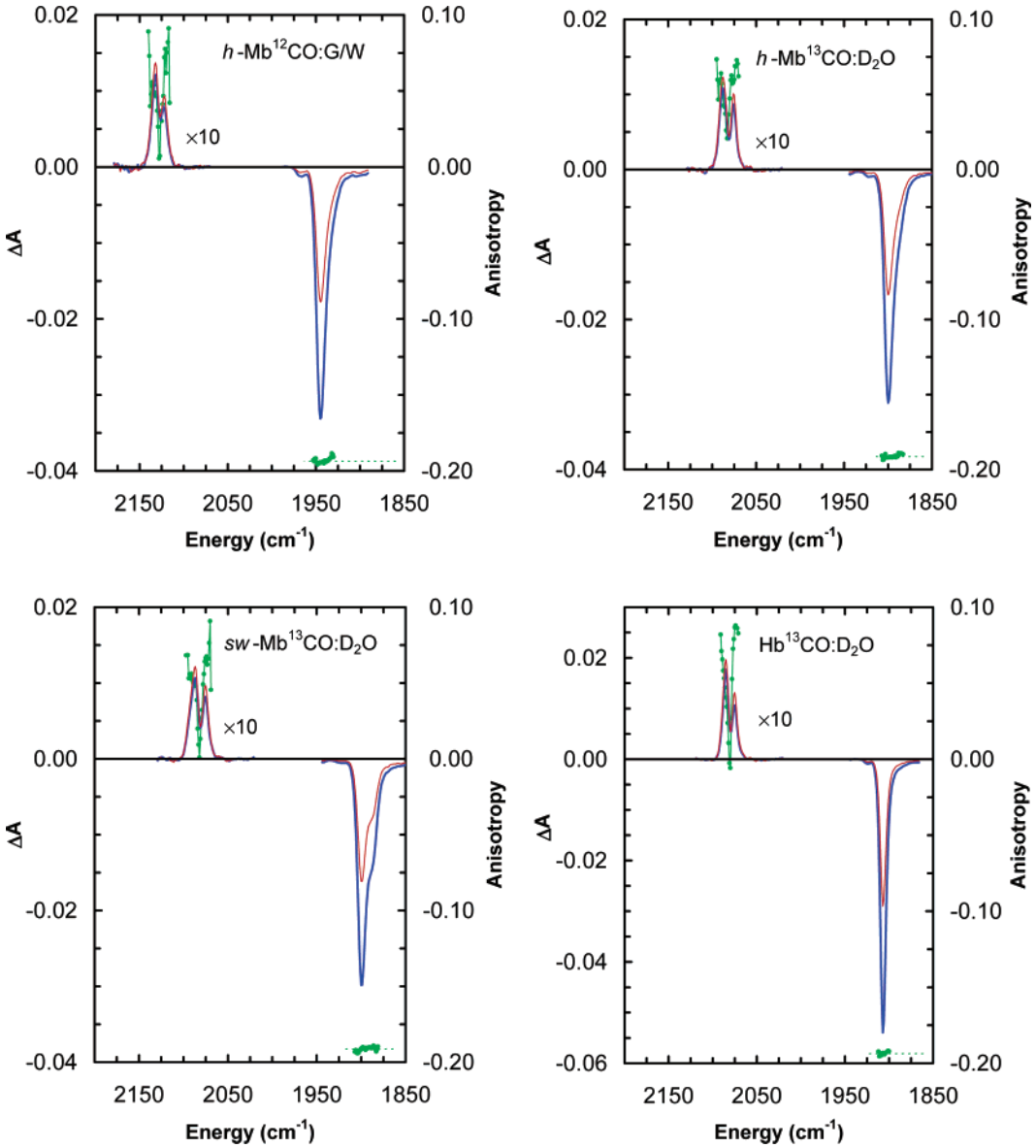


***Figure 4.*** Time-resolved polarized mid-IR absorbance spectra of photolyzed *h*-Mb$^{12}$CO:GW, *h*-Mb$^{13}$CO:D$_2$O, *sw*-Mb$^{13}$CO:D$_2$O, and Hb$^{13}$CO:D$_2$O. The *A*- and *B*-state spectra were recorded at ~10% and ~20% photolysis, respectively. The spectra were acquired with the pump pulse polarized perpendicular, $\Delta A^{\perp}$ (thick lines) and parallel, $\Delta A^{\parallel}$ (thin lines) to the probe pulse. The left ordinate depicts the pump-induced change in the absorbance of the sample and the right ordinate depicts the polarization anisotropy (filled circles). The polarization anisotropy corresponds to the anisotropy in the zero-photolysis limit, $r_{lim}$ (see text). The horizontal dashed lines represent the population-weighted average of the polarization anisotropy across the *A*-state features,

$$\langle r_{lim} \rangle = \sum_{\nu} \Delta A_{\nu}^{M} r_{lim,\nu} / \sum_{\nu} \Delta A_{\nu}^{M}$$

To compute $\langle r_{lim} \rangle$ for the *A*-states, the population was assumed to be proportional to the "magic" angle absorbance, $\Delta A^{M}$, computed at each energy, $\nu$, according to

$$\Delta A^{M} = \frac{(\Delta A^{\parallel} + 2\Delta A^{\perp})}{3}$$

Because the uncertainty in $r_{lim}$ becomes large when $\Delta A^{M}$ is small, the population-weighted average was confined to the range where $\Delta A^{M}$ was > 20% of its peak value. Because the absolute intensity of the CO absorbance decreases significantly upon dissociation from the heme, the *B*-state spectra have been scaled by ×10. For clarity, the background and hot band contributions to the *B*-state spectra have been removed.[16]

tional substates with different electrostatic fields in the vicinity of the active binding site. Calculations using density functional theory have suggested that hydrogen bonding interactions between bound CO and the distal histidine can account for the electrostatic effects nearly quantitatively.[43]

In the limit where the orientational probability distribution is a delta function in $\theta$, eq 2 can be used to calculate the angle of the CO transition dipole, the results of which are found in Table 1 under the heading $\langle \theta_{lim} \rangle$. Because the orientational probability distribution function is not a delta function, but has some nonzero width, $\langle \theta_{lim} \rangle$ represents an *upper limit* for the transition dipole of bound CO. To determine the equilibrium

(43) Franzen, S. *J. Am. Chem. Soc.* **2002**, *124*, 13 271−13 281.

***Table 1.*** *A*-State Polarization Anisotropy and the Orientation of the Bound CO Transition Dipole in MbCO and HbCO

| species | $\langle r_{lim} \rangle$[a] | $\theta_{lim}$ (deg)[b] | $\theta_{eq}$ (deg) |
|---|---|---|---|
| *h*-Mb$^{12}$CO:G/W | $-0.193_7 \pm 0.001_5$ | $8.3 \pm 1.0$ | $5.3 \pm 1.7$ |
| *h*-Mb$^{13}$CO:D$_2$O | $-0.191_4 \pm 0.001_0$ | $9.7 \pm 0.6$ | $7.4 \pm 0.8$ |
| *sw*-Mb$^{13}$CO:D$_2$O | $-0.191_8 \pm 0.001_2$ | $9.5 \pm 0.7$ | $7.0 \pm 0.9$ |
| Hb$^{13}$CO:D$_2$O | $-0.193_7 \pm 0.001_0$ | $8.3 \pm 0.7$ | $5.3 \pm 1.1$ |
| weighted average | $-0.192_5$ | 9.2 | 6.7 |

[a] $\langle r_{lim} \rangle$ is the population-weighted average of the anisotropy measured across the inhomogeneously broadened *A*-state spectra; it has been extrapolated to the limit of zero photolysis. [b] $\langle \theta_{lim} \rangle$ is the angle of the CO transition moment relative to the heme plane normal when P($\theta$) is modeled as a delta function. $\theta_{eq}$ is obtained by approximating an orientational distribution function $P(\theta)$ (see text).[16] The uncertainties reflect the statistical standard deviation of $r_{lim}$ across the *A*-state spectra.

orientation for the transition dipole, we need to know the functional form of the orientational probability distribution function, $P(\theta)$. We know of no direct measure of $P(\theta)$. Instead, we used the frequency of the axial Fe−C−O tilting mode in $Fe(CO)_5$[44] to estimate its bending force constant, from which an angular distribution function for axial-bound CO can be calculated. At 283 K, the Fe−C−O bending motion spans ± 4.5° (± estimated standard deviation of the angular distribution function), and the order parameter, *S*, for bound CO was estimated to be 0.98.[16] Given *S* and using eqs 2 and 5, the equilibrium orientation $\theta_{eq}$ of bound CO was determined for each sample (see Table 1). This correction suggests that the equilibrium orientation is only 2−3° smaller than the upper limit estimate obtained assuming $P(\theta)$ is a delta function. Of course, the potential of mean force for the Fe−C−O bending motion in MbCO and HbCO can differ from that for axial-bound CO in gas-phase $Fe(CO)_5$, and may require further revision of the CO orientation. However, the correction is already modest, so improvements in this estimate would not influence significantly our determination of $\theta_{eq}$.

The equilibrium orientation obtained after correcting for $P(\theta)$ is still an upper limit. Thermal motion of the heme and its surroundings causes the heme to deviate from planarity, thereby giving rise to a nonzero transition dipole along the direction of the heme normal. Because we do not know the magnitude of this transition dipole, we have not attempted to make a correction for an "ellipsoidal" heme absorber. Moreover, the heme can librate within the protein on a time scale that is fast compared to the 100 ps time delay of our measurement.[45] This motion causes a time-dependent decay of the measured anisotropy, the magnitude of which is related to the amplitude of the heme librational motion. According to MD simulations performed on MbCO in vacuo by Henry,[45] the heme motion causes the anisotropy to decay approximately 1.5% by 100 ps. Because the simulations were performed in vacuo, the loss of anisotropy would be expected to be smaller for proteins in solution. This expectation stems from the fact that conformational dynamics of proteins are coupled to, and slowed by, the surrounding solvent.[46−48] Hochstrasser and co-workers[49] explored this issue experimentally by measuring the polarization anisotropy of HbCO from 350 fs to 1 ns, which they found to be time-independent within their estimated experimental uncertainty of ± 3%. Consequently, they concluded that the heme orientation is fairly rigidly constrained within a protein. Note that a 1.5% correction to the *h*-Mb$^{12}$CO:G/W anisotropy is sufficient to reduce $\theta_{eq}$ from 5.3° to 0.

Aside from systematic errors that can be introduced when measuring the polarization anisotropy,[50] all factors that influence the polarization anisotropy tend to reduce its absolute value. The corrections that we have made, plus those we have not, demonstrate that the transition moment for bound CO is oriented ≤9° from the heme plane normal and may be as small as 0°.

Using a technique referred to as infrared crystallography, Sage and co-workers found that the transition dipole for $A_1$ and $A_3$ are both consistent with $\theta = 6.7° \pm 0.9°$ and $\phi = 69° \pm 8°$.[51] The technique of vibrational crystallography involves measuring polarized IR absorbance spectra along different principle crystallographic directions on different faces of crystals belonging to different point groups (e.g., $P2_1$ and $P2_12_12_1$), from which the projection of the CO transition dipole onto the heme normal can be uniquely determined in $\theta$ as well as $\phi$. Their agreement with our previously reported determination[17] and the results presented here is striking considering the measurements were made on proteins in crystals vs in solution. This agreement suggests that the active site is unperturbed by crystal packing forces in $P2_1$ and $P2_12_12_1$, at least from the perspective of the bound CO.

Whereas these spectroscopic measurements determine the orientation of the CO transition dipole, what we are really after is the orientation of the C−O bond. When CO is dissociated from the heme, the transition dipole is parallel to the C−O bond axis. However, binding to the heme causes a 10% red shift of the CO vibrational frequency and a more than 10-fold increase of its oscillator strength. Consequently, its transition dipole must be delocalized across the Fe−C−O bonds, and the direction vector of the transition dipole can differ from the C−O bond direction. Spiro and co-workers addressed this issue theoretically with gradient-corrected density functional theory.[52] They calculated the C−O transition dipole direction for various Fe−C−O bend and tilt geometries along the minimum energy path. They found that a 6.9° transition dipole corresponds to a minimum energy structure with the Fe−C−O bent 5.8° and the Fe−C bond tilted 9.5° (relative to the heme normal). Consequently, our spectroscopic determination of the transition dipole is consistent with a C−O angle less than 15.3° from the heme normal. A 1.15 Å resolution MbCO crystal structure,[53] determined by Bartunik and co-workers, was modeled with the Fe−C−O bent 7.4°± 1.9°, the Fe−C bond tilted 4.7°± 0.9°, and the C−O orientation 12.1° from the heme normal. Schlichting and co-workers[1] also reported a structure at 1.15 Å resolution, and modeled their data with the Fe−C−O bent 9°± 3°, the Fe−C bond tilted 9°, and the C−O orientation at 18°± 3°. A "unified" model based on nmr, Mossbauer and infrared spectroscopies concluded that the Fe−C−O geometry is bent 7° and

(44) Pistorius, C. W. F. T.; Haarhoff, P. C. *J. Chem. Phys.* **1959**, *31*, 1439−1443.
(45) Henry, E. R. *Biophys. J.* **1993**, *64*, 869−885.
(46) Ansari, A.; Jones, C. M.; Henry, E. R.; Hofrichter, J.; Eaton, W. A. *Science* **1992**, *256*, 1796−1798.
(47) Lim, M.; Jackson, T. A.; Anfinrud, P. A. *Proc. Natl. Acad. Sci. U.S.A.* **1993**, *90*, 5801−5804.
(48) Jackson, T. A.; Lim, M.; Anfinrud, P. A. *Chem. Phys.* **1994**, *180*, 131−140.
(49) Locke, B.; Lian, T.; Hochstrasser, R. M. *Chem. Phys.* **1991**, *158*, 409−419.
(50) Locke, B.; Lian, T.; Hochstrasser, R. M. *Chem. Phys.* **1995**, *190*, 155.
(51) Sage, J. T.; Jee, W. *J. Mol. Biol.* **1997**, *274*, 21−26.
(52) Spiro, T. G.; Kozlowski, P. M. *J. Am. Chem. Soc.* **1998**, *120*, 4524−4525.
(53) Kachalova, G. S.; Popov, A. N.; Bartunik, H. D. *Science* **1999**, *284*, 473−476.

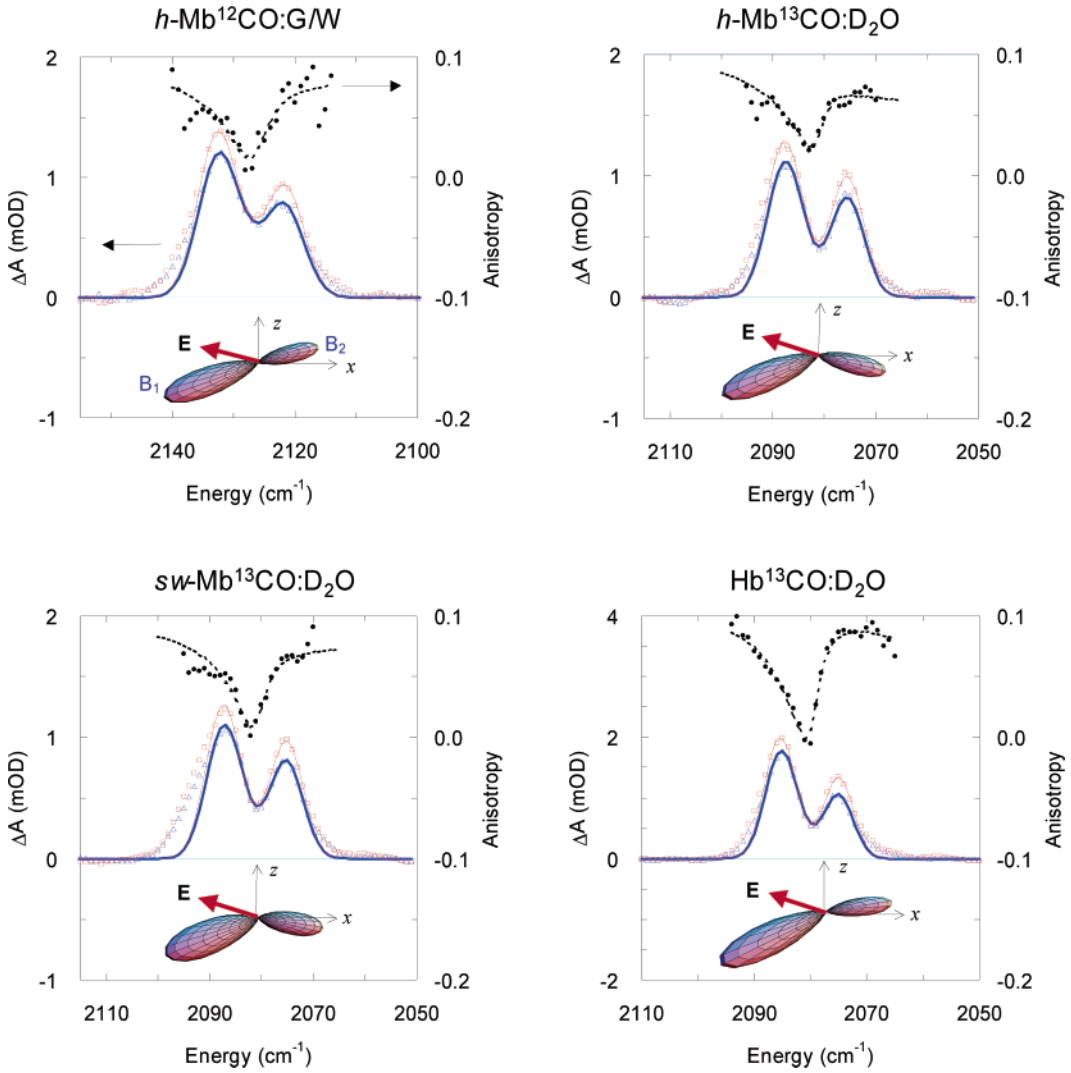


***Figure 5.*** Expanded views of polarized *B*-state spectra shown in Figure 4. The anisotropies were extrapolated to zero photolysis (see text). The solid lines correspond to a simple model based on a double well cosine potential for the CO orientation; the least-squares optimization was confined to the region where the absorbance is greater than 30% of its neighboring peak. Except for the wings of the spectra, the absorbance and anisotropy features are reproduced with high fidelity (see text). The best-fit orientational probability distribution functions are plotted as 3-D rendered objects with the Stark field found in the *xz*-plane.

tilted 4°.[54] The discrepancies among the C−O angle are all within a few degrees, and all determinations conclude that the CO orientation is only modestly displaced away from the heme normal, a perturbation too small to account for physiological discrimination between CO and $O_2$. Moreover, the results reported here shows that the geometry of *bound* CO is virtually the same for MbCO (horse and sperm whale) and HbCO, and is unchanging across their inhomogeneously broadened mid-IR absorption spectra. Evidently, discrimination between CO and $O_2$ in Mb and Hb resides not so much in a steric perturbation to the binding geometry of CO, but in the strength of the hydrogen bonding interactions between the bound ligand and the histidine.[55−57]

**4.4 B-State Anisotropy: Orientation of Docked CO.** The *B*-state spectra of photolyzed *h*-MbCO, *sw*-MbCO, and HbCO (see Figure 5) all reveal two well-resolved features, as reported earlier.[16] These features are similar to those produced by photolysis of *sw*-MbCO at 5.5 K[40] where the larger feature was denoted $B_1$ and the smaller one $B_2$. The wavelength dependence of the *B*-state polarization anisotropy is similar among *h*-Mb (in $D_2O$ and G/W), *sw*-Mb, and Hb, with the anisotropy maximized near the outermost wings of $B_1$ and $B_2$ and minimized near the midpoint between the two features. The minimum anisotropy in each measurement is approximately zero and occurs near the midpoint of the two features, suggesting that the trajectory for interconversion between $B_1$ and $B_2$ causes CO to sweep through a polar angle around 54.7° (the so-called magic angle where the anisotropy becomes zero), at which point the CO-orientation is nearly orthogonal to the Stark field.

The experimentally observed polarized *B*-state spectra and anisotropy are qualitatively similar to the model function shown in Figure 2a (calculated using Equation 4 with $\theta_1 = \theta_2 = \pi/2$ and $\phi_1 - \phi_2 = \pi$), where the equilibrium orientation of CO is parallel to both the heme plane and the Stark field. A least-squares optimization of the model parameters was carried out

(54) McMahon, M. T.; deDios, A. C.; Godbout, N.; Salzmann, R.; Laws, D. D.; Le, H.; Havlin, R. H.; Oldfield, E. *J. Am. Chem. Soc.* **1998**, *120*, 4784−4797.
(55) Pauling, L. *Nature* **1964**, *203*, 182.
(56) Springer, B. A.; Sligar, S. G.; Olson, J. S.; Phillips, G. N., Jr. *Chem. Rev.* **1994**, *94*, 699−714.
(57) Spiro, T. G.; Kozlowski, P. M. *Acc. Chem. Res.* **2001**, *34*, 137−144.

***Table 2.*** Least-Squares Fit Parameters Obtained When Modeling the *B*-State Spectra in Figure 5

| | bandwidth | Stark field | | | orientational direction ($\theta_{eq}$) | | potential (kJ/mol) | |
|---|---|---|---|---|---|---|---|---|
| sample | fwhm ($cm^{-1}$) | $\mathbf{E}\cdot\Delta\mu$ ($cm^{-1}$) | $\theta_E$ (deg)[a] | solvation ($cm^{-1}$) | $B_1$ (deg)[a] | $B_2$ (deg)[a] | $\Delta$ | barrier |
| h-Mb$^{12}$CO:G/W | 4.7 | 7.8 | 64 (116) | −15.9 | 113 (67) | 74 (106) | 1.1 | 17.5 |
| h-Mb$^{13}$CO:$D_2O$ | 4.9 | 7.8 | 64 (116) | −13.3 | 112 (68) | 104 (76) | 0.9 | 14.8 |
| sw-Mb$^{13}$CO:$D_2O$ | 4.8 | 7.5 | 73 (107) | −14.1 | 112 (68) | 100 (80) | 1.0 | 10.6 |
| Hb$^{13}$CO:$D_2O$ | 3.6 | 8.1 | 59 (121) | −14.9 | 116 (64) | 83 (97) | 1.4 | 19.6 |
| Average | 4.5 | 7.8 | 65 (115) | −14.6 | 113 (67) | 90 (90) | 1.1 | 15.6 |

[a] Parameters in parentheses are equivalent by symmetry (see text). The model assumes CO is constrained by a double-well potential (eq 4) bathed in a Stark field. fwhm is the modeled line width for a Gaussian in the absence of Stark field. "Solvation" is the difference between the vibrational frequencies of CO in the gas phase and in the docking site (in the absence of Stark field). The potential barrier separating the equilibrium orientation of CO in the two wells is calculated from the fitted parameter $V_0$ in eq 4, and $\Delta$ is the energy separation between the two minima.

with the *B*-state spectra and the anisotropy fit simultaneously, the results of which are plotted in Figure 5 and tabulated in Table 2. Nine parameters were used in each fit including a scale factor, $V_0$, "Solvation" parameter, $B_1$ and $B_2$ well separation, $\Delta$, spectral fwhm, the product $\mathbf{E}\cdot\Delta\mu$, and three equilibrium theta angles: $\theta_E$, $\theta_{B1}$, and $\theta_{B2}$. The parameter denoted $V_0$ controls the steepness of the potential and affects the potential barrier separating $B_1$ and $B_2$, the magnitude of which was determined numerically and denoted "Barrier" in Table 2. The energy difference between the two minima, $\Delta$, controls the relative population of $B_1$ and $B_2$. The "Solvation" parameter corresponds to the protein-induced shift of the CO vibrational frequency (relative to the gas phase) in the absence of a Stark field. The fwhm corresponds to the modeled line width of $B_1$ and $B_2$ in the absence of a Stark field (assuming a Gaussian line shape). The product $\mathbf{E}\cdot\Delta\mu$ is the maximum Stark shift (corresponding to CO aligned with the Stark field). The theta angles correspond to the angle between the equilibrium orientation and the heme normal (see Figure 1a). At the outset, both polar angles ($\theta$, $\phi$) for the equilibrium orientations of $B_1$ and $B_2$ were optimized; however, the two lobes converged to opposite orientations ($\phi = 0°$ vs 180°) in the same plane as the **E**-field vector (the azimuthal angle of the **E**-field vector had been set to zero with no loss of generality), so the final refinement was performed with the direction vectors for the lobes and the E-field confined to the *xz*-plane (equivalent to the *yz*-plane).

This minimalist model does a remarkably good job of reproducing the experimental data over most of the spectra, except for in the wings. It is well-known that conformational substates in *sw*-MbCO lead to multiple vibrational *A*-states.[40] This conformational heterogeneity likely affects the *B*-states as well, and may account for the asymmetric shape of $B_1$ in photolyzed *sw*-MbCO. It has been pointed out that *h*-MbCO suffers less from this conformational heterogeneity,[58] and may explain why *h*-Mb·CO is modeled more accurately than *sw*-Mb·CO with this simple model. Consistent with this view is the observation that the IR spectrum of HbCO is dominated by a single *A*-state, and its *B*-states are modeled even more accurately than those in *h*-Mb·CO. Rather than increase the complexity of the model to deal with conformational heterogeneity, we elected to confine the range over which the data were fit to the region where the absorbance is greater than 30% of its neighboring peak. As can be seen in Figure 5, the fitted curves over this range reproduce the data with high fidelity, and deviate from the experimental data only in the wings, which represent a minority population.

Most of the best-fit parameters, summarized in Table 2, are similar among the heme proteins investigated. The fwhm of the "field-free" Gaussian line shape is about 4.8 $cm^{-1}$ for all Mb samples, but is 3.6 $cm^{-1}$ for Hb, reflecting the narrower line width found in photolyzed HbCO.[16] The direction of the Stark field varies modestly, ranging from 59° to 73°. The equilibrium orientation of $B_1$ is 113° with negligible dispersion across the series, while the equilibrium orientation of $B_2$ is within 15° of the heme plane, and averages 90°. Assuming $B_1$ and $B_2$ are in thermodynamics equilibrium, their enthalpy difference (deduced from their relative population) is ∼1 kJ/mol in Mb and 1.4 kJ/mol in Hb. Being more stable, the $B_1$ state is represented by the larger lobe in the 3-D rendered object in Figure 5. Evidently, the interactions that stabilize $B_1$ relative to $B_2$ are slightly stronger in Hb than in Mb, perhaps accounting for the narrower spectral features observed. The vibrational frequency of "docked" CO is shifted from its gas-phase value by an amount that varies somewhat across the series. The largest difference appears to be a solvent effect: when dissolved in a glycerol/water mixture, the vibrational frequency of "docked" CO in *h*-MbCO is red-shifted 2.5 $cm^{-1}$ relative to its $D_2O$ value. Because the docking site is confined within the hydrophobic interior of the protein, this effect should not be a dielectric effect, but likely arises from a glycerol-induced perturbation of the protein structure. The magnitude of the red shift (∼15 $cm^{-1}$) seems large compared to the 10 $cm^{-1}$ red-shift observed for CO in benzene matrixes at 30 K[59] or the 5 $cm^{-1}$ red-shifts observed in liquid CO at 69K and solid CO at 59 K.[60] However, this red shift is comparable to that observed for CO in $D_2O$, in glycerol/water mixtures, and when trapped in other hydrophobic cavities inside Mb.[61] The magnitude of the interaction between the Stark electric field and the Stark tuning rate, $\mathbf{E}\cdot\Delta\mu$, is 7.8 $cm^{-1}$ in *h*-Mb, and differs by only a few tenths of a wavenumber in *sw*-Mb and Hb. Evidently, the electrostatic environment in the vicinity of the docking site is highly conserved in Mb and Hb. The "Barrier" estimates in Table 2 correspond to the activation barrier for end-to-end rotation. In an absolute sense, these estimates cannot be taken too seriously because the cylindrically symmetric double-well potential is a simple approximation to a more complex multidimensional surface; however, the trends suggest that the activation barrier is larger in Hb and in Mb when dissolved in a glycerol/water mixture. Given the narrower *B*-state spectra in Hb and its greater rigidity due to quaternary contacts between the alpha and beta chains, it would not be surprising to have a more tightly constrained "docked" CO

(58) Nienhaus, G. U.; Mourant, J. R.; Chu, K.; Frauenfelder, H. *Biochemistry* **1994**, *33*, 13 413−13 430.
(59) Jiang, J. J.; Person, W. B.; Brown, K. G. *J. Chem. Phys.* **1975**, *62*, 1201−1211.
(60) Ewing, G. E. *J. Chem. Phys.* **1962**, *37*, 2250−2256.
(61) Jackson, T. A. Ph.D. Thesis; Harvard University: Cambridge, MA, 1996.

orientation. Moreover, because protein dynamics are slaved to the solvent,[48,62,63] raising the solvent viscosity by adding glycerol would be expected to slow internal motion and give rise to a larger apparent barrier.

The measurements reported here cannot identify where in the heme pocket the CO is located, only how it is oriented. Moreover, because our measurements determine the magnitude of a vector's projection onto the heme normal, there are two symmetrically equivalent sets of theta angles that are consistent with our data. The second set is enclosed in parentheses in Table 2. Because polarization spectroscopy cannot distinguish between these two configurations, additional information is needed to make that assignment. Earlier ultrafast mid-IR measurements characterized the appearance of $B_1$ and $B_2$ and reported time constants of 200 and 500 fs, respectively, demonstrating that the location of the docking site must be near the binding site, with $B_1$ possibly residing closer to the heme.[18] According to molecular dynamics (MD) simulations by Karplus and coworkers, CO is constrained in an L-shaped thin slab containing two higher probability regions with its bond axis nominally aligned parallel to the heme plane at a distance 3.2 ± 0.3 Å above the plane.[64] They found that CO localized in the nearer region, found 1.3 Å from the heme normal, has an equilibrium orientation of about 125° with the O atom pointing downward toward the iron. The orientational preference for the O atom to point toward the iron atom has been attributed to a nonbonded electrostatic interaction of CO with the heme, the distal histidine and the proximal histidine, as well as van der Waals interaction with the heme and the distal histidine.[64] When CO is localized in the more distant region, found 2.3 Å from the heme normal, it is oriented at 90°. These locations are consistent with the CO docking sites found in low-temperature crystallography measurements.[1−4] It is tempting to assign $B_1$ to the nearer of the two regions in the L-shaped cavity. With this assignment, the ∼113° and ∼90° orientations found in this work for $B_1$ and $B_2$ correlate nicely with the ∼125° and ∼90° orientations found for the 1.3 and 2.3 Å high probability sites in the MD simulations.[64] These states interconvert rather freely, with ligand binding likely proceeding through $B_1$, the region nearer the heme iron. One possible interconversion trajectory that is consistent with the L-shaped cavity and our anisotropy data involves a simple motion where the C end of CO acts as a pivot point near the corner of the L-shaped region while the O end flips through a polar angle around 54.7° from one arm of the planar cavity toward the other. It would be interesting to explore this hypothesis in further detail through MD simulations. If $B_1$ corresponds to CO with its slightly positively charged O end pointing toward the iron, then the ligand is far from the transition state for rebinding, and would be expected to rebind slowly, as has been observed.[13−15] If NO accessed that site with its positively charged N atom pointing toward the iron, it would be close to the transition state for rebinding and should exhibit rapid NO geminate rebinding, as has been observed.[65−67] By extension, the rebinding rate of $O_2$, which is neutral and binds with a bent geometry, would be between those of CO and NO, as has been observed.[67−69] The hypothesis that $B_1$ and $B_2$ correspond to spectra from adjacent sites in the heme pocket as described above can, in principle, be tested in a mid-IR MbNO rebinding experiment, where the fast geminate rebinding should lead to a sequential decrease of these spectral amplitudes.

Given the product $\mathbf{E}\cdot\Delta\mu \approx 7.8$ cm$^{-1}$ and a theoretical estimate of the Stark tuning rate $\Delta\mu \cong 67$ cm$^{-1}$(V/Å)$^{-1}$,[26] the magnitude of the electric field at the CO docking site can be estimated to be ∼0.12 V/Å. The potential gradient for a model heme-imidazole group has been calculated using ab initio methods,[30] and estimated to be approximately 0.2 V/Å in the vicinity of the docking site. The similar magnitude of these two estimates of the electric field suggests that the heme-imidazole group dominates the electrostatic environment in the vicinity of the primary ligand docking site.

Might the correlation between the vibrational frequency and the polarization anisotropy have some origin other than a Stark shift? A correlation between vibrational frequency and C−O orientation might arise from specific interactions between CO and the residues that fashion the docking site, e.g., hydrogen bonding with a protonated distal histidine.[70] Using ab initio methods, Straub and Karplus[70] calculated the vibrational frequency shift that would be observed if CO were H-bonded to a protonated imidazole. They calculated a 36 cm$^{-1}$ blue shift when the C end of CO was H-bonded and a 17 cm$^{-1}$ red shift when the O end was H-bonded.[70] The magnitude of these shifts are of the same order as the 24 cm$^{-1}$ blue shift observed for the CO vibrational stretch of gas-phase OC—HF.[71] It would appear that these shifts are far too large to account for the experimentally observed Stark shift (∼7.8 cm$^{-1}$). Moreover, the distance between the distal histidine and docked CO is beyond normal H-bonding distance (according to a cryo-crystallography structure determination, the epsilon nitrogen of the distal histidine is 3.9 Å from the nearest atom of "docked" CO[6]). Consequently, the splitting of the two *B*-states appears to be dominated by a Stark field, but may be modified somewhat by specific interactions between CO and the neighboring residues.

It is quite remarkable that CO located so close to the binding site rebinds so slowly. Evidently, what matters most is how the CO is oriented as it approaches the heme iron. Because we see no CO oriented at an angle less than about 54.7° (corresponding to a measured anisotropy of zero), we conclude that access to the transition state for rebinding is a rare event. This conclusion is supported by MD simulations[25,64] and low-temperature crystallography measurements[1−4] which find that an upright orientation with the C end of CO pointing toward the iron is quite rare, especially when the CO approaches the heme iron

## 5. Conclusions

The orientational probability distribution function for CO transiently docked in Mb and Hb has been determined experimentally for the first time. The ellipsoids are quite similar for all protein systems investigated, demonstrating that the highly

(62) Hagen, S. J.; Hofrichter, J.; Eaton, W. A. *Science* **1995**, *269*, 959−962.
(63) Fenimore, P. W.; Frauenfelder, H.; McMahon, B. H.; Parak, F. G. *Proc. Natl. Acad. Sci. U.S.A.* **2002**, *99*, 16 047−16 051.
(64) Vitkup, D.; Petsko, G. A.; Karplus, M. *Nat. Struct. Biol.* **1997**, *4*, 202−208.
(65) Cornelius, P. A.; Hochstrasser, R. M.; Steele, A. W. *J. Mol. Biol.* **1983**, *163*, 119−128.
(66) Petrich, J. W.; Lambry, J.-C.; Balasubramanian, S.; Lambright, D. G.; Boxer, S. G.; Martin, J. L. *J. Mol. Biol.* **1994**, *238*, 437−444.
(67) Petrich, J. W.; Poyart, C.; Martin, J. L. *Biochemistry* **1988**, *27*, 4049−4060.
(68) Greene, B. I.; Hochstrasser, R. M.; Weisman, R. B.; Eaton, W. A. *Proc. Natl. Acad. Sci. U.S.A.* **1978**, *75*, 5255−5259.
(69) Chernoff, D. A.; Hochstrasser, R. M.; Steele, W. A. *Proc. Natl. Acad. Sci. U.S.A.* **1980**, *77*, 5606−5610.
(70) Straub, J. E.; Karplus, M. *Chem. Phys.* **1991**, *158*, 221−248.
(71) Zhongcheng, W.; Bevan, J. W. *J. Chem. Phys.* **1989**, *91*, 3335−3339.

conserved residues surrounding the heme in Mb and Hb fashion a docking site that performs a common function. When CO is trapped within this docking site, rotation out of the heme plane is hindered, a fact that has important consequences for geminate rebinding dynamics. For example, to rebind to the heme iron, the CO must access the transition state for binding, an orientation with CO aligned near the heme plane normal. Consequently, the orientational and spatial constraints imposed on CO by the docking site strongly hinder CO binding, and facilitate the excretion of this toxic ligand. This feat is quite remarkable considering the ligand is so small, is docked only ∼2 Å away from the binding site, and undergoes substantial thermal motion at room temperature. Clearly, the highly ordered protein structure surrounding the active site of an enzyme confers upon it exquisite selectivity, even for small ligands.

**Acknowledgment.** M. Lim acknowledges support for this work by Korea Research Foundation Grant (KRF-2001-015-DP0228). We thank John Olson for providing a sample of *sw*-MbCO.

JA035475F